

## Coupled thermoelasticity of a functionally graded cracked layer under thermomechanical shocks

M. M. ROKHI, M. SHARIATI

*Department of Mechanical Engineering  
Shahrood University of Technology  
Shahrood, Iran  
e-mail: masoud\_mahdizadeh@yahoo.com*

THIS PAPER INVESTIGATES LINEAR-ELASTIC RESPONSE of cracked functionally graded layers subjected to thermomechanical loading; classical coupled thermoelastic equations are used in the calculations. The coupled dynamical system of equations obtained from the extended finite element discretization is solved by the Newmark method in the time domain. Micromechanical models for conventional composites are used to estimate properties of functionally graded layer. The interaction integral is then employed to calculate the stress intensity factors at each time step. In addition, crack propagation phenomenon under thermomechanical shocks is investigated in this paper. We have used MATLAB software to implement the algorithm and related code of problem.

**Key words:** coupled thermoelasticity, fracture, crack propagation, FGMs, thermomechanical shocks.

Copyright © 2013 by IPPT PAN

### 1. Introduction

FUNCTIONALLY GRADED MATERIALS (FGMs) are a new class of composite materials characterized by the gradual variation in microstructure and material properties. FGMs were initially designed as thermal barrier materials for aerospace structural applications and fusion reactors. They are now developed for general use as structural components in extremely high-temperature environments. FGM components are generally constructed to sustain severe temperature gradients. Ceramic materials, because of their excellent properties at high temperatures and their superior wear and corrosion resistance, are used widely in making of FGMs. One major limitation of ceramics is their intrinsic brittleness that can result in fracture under severe thermal shocks. Therefore, the fracture analyses of FGMs under thermal shocks are important for their durability in engineering applications.

To adapt the standard finite element method to the fracture computations, the extended finite element method (XFEM) has been developed, which completely avoids remeshing [1–3]. This XFEM is based on the partition of unity [4].

In this method, a discontinuous enrichment function is used along the crack path in order to describe a discontinuous displacement [2]. BELYTSCHKO *et al.* [5] developed the method for dynamic crack growth with a loss of hyperbolicity as a propagation criterion. ROZYCKI *et al.* [6] studied the critical time step within XFEM in explicit dynamic crack propagation with enrichment kept active during the propagation. LINDER and ARMERO [7] have treated dynamic crack propagation with embedded discontinuity elements. MENOILLARD *et al.* [8] presented a new method for crack tip enrichment based on allowing the enrichment to be a function of time.

The response of functionally graded cracked layers under thermomechanical shocks is found in just a few articles. NODA [9] and FUJIMOTO and NODA [10, 11] conducted a series of researches on using the finite element method to obtain the crack SIFs under thermal loading conditions in the homogeneous and functionally graded materials. They considered the heat conduction equation where thermo-coupling has been ignored. JIN and PAULINO [12] studied an edge crack in a strip of a functionally graded material under transient thermal loading conditions. They employed a multi-layered material model to obtain the temperature field. Without considering the thermoelastic coupling effect, transient elastodynamic crack analyses in functionally graded materials have been presented previously by many researchers in literature using various methods (see [13, 14] for more references cited therein). HOSSEINI-TEHRANI and ESLAMI [15] and HOSSEINI-TEHRANI *et al.* [16] employed the boundary element method to investigate the effect of the coupling and inertia terms in dynamical thermal loading problems. DUFLOT [17] investigated the static case of thermoelastic fracture by the XFEM where both 2D and 3D problems with different crack face thermal boundary conditions are included. KC and KIM [18] using the finite element method evaluated the non-singular T-stress and mixed-mode stress intensity factors in FGMs under steady-state thermal loads via interaction integral. WANG and QIN [19] developed a meshless algorithm based on analog equation theory to simulate the static thermal stress distribution in two-dimensional FGMs. ZAMANI and ESLAMI [20] employed the finite element method to obtain the SIF for a functionally graded cracked body under coupled classical thermoelastic assumption. They assumed that the crack remains stationary within simulation. Also the XFEM formulation was implemented by ZAMANI and ESLAMI [21] to model the effect of the mechanical and thermal shocks on a cracked body. The crack was assumed to be stationary. FENG and JIN [22] examined the fracture behavior of an FGM plate containing parallel surface cracks with alternating lengths subjected to a thermal shock. EKHLAKOV *et al.* [23] developed a boundary-domain element method (BDEM) for a transient thermoelastic crack analysis in isotropic, continuously non-homogeneous and linear elastic FGMs. They considered a stationary edge crack in a two dimensional finite domain subjected to a thermal shock and com-

puted stress intensity factors. In addition, they performed a transient thermoelastic crack analysis in two-dimensional, isotropic, continuously non-homogeneous and linear elastic FGMs subjected to a thermal shock using the Laplace transform technique and the boundary element method [24]. They investigated the influences of the material gradation, thermo-mechanical coupling, crack orientation and thermal shock loading on the dynamic stress intensity factors for stationary cracks.

The study of crack propagation phenomena in a functionally graded cracked layer under thermomechanical shocks using the coupled thermoelastic equations and the XFEM have not been investigated in the previous studies. In the present study, the XFEM formulation is implemented to model the effect of thermal shocks on a functionally graded cracked layer under coupled classical thermoelastic assumption. The Newmark time-integration scheme is used to solve the dynamical system of matrix equations obtained from the spatial discretization of initial coupled equations. The most general form of interaction integral for FGMs is extracted based on the non-equilibrium formulation and the dynamical stress intensity factors are computed in each time step. A MATLAB code is developed to implement the different stages of computation from mesh generation to calculation of SIFs and crack propagation simulation. Some numerical examples are implemented to investigate the validity and accuracy of the written computer program. The effects of volume fraction profiles of FGMs on SIFs are investigated in this paper. The crack is assumed to be moving under thermal and mechanical shocks. In addition, crack propagation phenomenon is considered which seems not to be reported with this condition in previous works.

## 2. General problem formulation

### 2.1. Governing equations

The general governing equations of the classical coupled thermoelasticity are the equation of motion (Eq. (2.1)) and the first law of thermodynamics (Eq. (2.2)), as [25],

$$(2.1) \quad \sigma_{ij,j} + B_i = \rho \ddot{u}_i,$$

$$(2.2) \quad q_{i,i} + \rho c_t \dot{\theta} + T_0(1 + \theta/T_0)\beta \dot{\epsilon}_{ii} = R,$$

where  $\sigma_{ij}$ ,  $B_i$ ,  $u_i$  and  $q_i$  are components of the stress tensor, components of the body force vector, components of the displacement vector and components of the heat flux vector per unit area respectively. Also  $\rho$  is the density,  $c_t$  is the specific heat capacity,  $R$  is the generated heat per unit volume,  $\beta = \alpha(3\lambda + 2\mu)$ ,  $\alpha$  is the coefficient of thermal expansion and  $\theta = (T - T_0)$ . If the temperature

change  $\theta$  is small compared to the reference temperature  $T_0$ , Eq. (2.2) may be approximately written in the simpler form [25]

$$(2.3) \quad q_{i,i} + \rho c_t \dot{\theta} + T_0 \beta \dot{\varepsilon}_{ii} = R.$$

Hooke's law correlates the stress tensor to the displacement components and temperature change  $\theta$  via Eq. (2.4)

$$(2.4) \quad \sigma_{ij} = \mu(u_{i,j} + u_{j,i}) + [\lambda u_{k,k} - \beta \theta] \delta_{ij},$$

where  $\mu$  and  $\lambda$  are Lamé's constants and they vary with spatial location in FGMs. According to Fourier's law of heat conduction we have:

$$(2.5) \quad q_i = -k_{ij} \theta_{,j},$$

here  $k_{ij}$  is the coefficient of thermal conduction for a general anisotropic material and it varies with spatial location in FGMs.

## 2.2. Space discretization

The system of coupled equations (2.1) and (2.2) does not have a general analytical solution. The extended finite element model of the problem is obtained by discretizing the solution domain into a number of arbitrary elements. In the XFEM formulation, a standard local displacement approximation around the crack is enriched with discontinuous jump function across the crack faces and the asymptotic crack tip displacement field around the crack tip [1]. The same procedure is used for the temperature enrichment [17]. The formulation of the XFEM for displacement components can be written as [21],

$$(2.6) \quad \mathbf{u}(x, y, t) = \sum_{\text{all nodes}} N_n(x, y) \mathbf{a}_n(t) + \sum_{n \in N_{\text{cr}}} N_n(x, y) [H(x, y) - H(x_n, y_n)] \mathbf{b}_n(t) \\ + \sum_m \sum_{n \in N_{\text{tip}}} N_n(x, y) [F_m(r, \varphi) - F_m(r_n, \varphi_n)] \mathbf{c}_{nm}(t),$$

where  $N_{\text{cr}}$  is the set of nodes that the discontinuity has in its influence domain, while  $N_{\text{tip}}$  is the set of nodes inside a predefined area around the crack tip (see Fig. 1). Here,  $H(x, y)$  is Heaviside enrichment function and  $F_m$  represents crack tip enrichment functions [26]. Also

$$\mathbf{a}_n(t) = \{a_n^u(t), a_n^v(t)\}^T, \quad \mathbf{b}_n(t) = \{b_n^u(t), b_n^v(t)\}^T, \quad \mathbf{c}_{nm}(t) = \{a_{nm}^u(t), a_{nm}^v(t)\}^T$$

are vectors of the nodal unknowns.

In this study, the crack faces are assumed to be adiabatic so the temperature is discontinuous along the crack faces and the heat flux is singular at the crack tip.

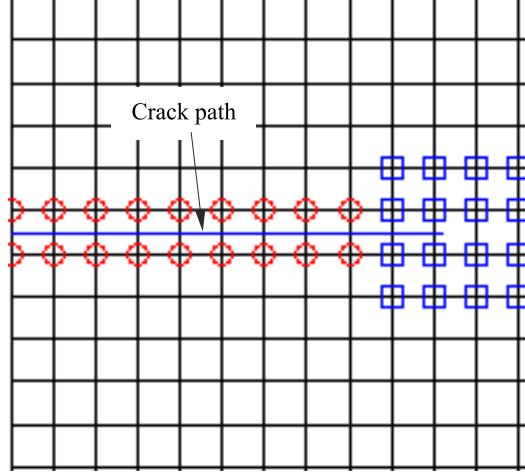


FIG. 1. Selection of enriched nodes for edge crack. Circled nodes are enriched by the discontinuity function whereas the squared nodes are enriched by the crack tip enrichment functions.

Thus, the temperature field is discretized similar to the displacement field, but only with the one crack tip enrichment function [21]

$$\begin{aligned}
 (2.7) \quad \theta(x, y, t) = & \sum_{\text{all nodes}} N_n(x, y) a_n^T(t) \\
 & + \sum_{n \in N_{cr}} N_n(x, y) [H(x, y) - H(x_n, y_n)] b_n^T(t) \\
 & + \sum_{n \in N_{tip}} N_n(x, y) [r^{0.5} \sin(\varphi/2) - r_n^{0.5} \sin(\varphi_n/2)] c_n^T(t),
 \end{aligned}$$

where  $r$  and  $\varphi$  are the usual crack-tip polar coordinates. Also  $a_n^T(t)$ ,  $b_n^T(t)$  and  $c_n^T(t)$  are nodal unknowns corresponding to temperature field. Now, the base element ( $e$ ) with  $n$  nodal points is considered and the displacement components and the temperature change in the element ( $e$ ) are approximated by compact forms as follows:

$$(2.8) \quad u^e(x, y, t) = N_h(x, y) a_h^u(t) + \Phi_h(x, y) b_h^u(t) + \Psi_{hm}(x, y) c_{hm}^u(t),$$

$$(2.9) \quad v^e(x, y, t) = N_h(x, y) a_h^v(t) + \Phi_h(x, y) b_h^v(t) + \Psi_{hm}(x, y) c_{hm}^v(t),$$

$$(2.10) \quad \theta^e(x, y, t) = N_h(x, y) a_h^T(t) + \Phi_h(x, y) b_h^T(t) + \Psi_{hm}(x, y) c_{hm}^T(t),$$

$h = 1, 2, \dots, ne$ ,  $m = 1, 2, 3, 4$ , where  $ne$  is the number of nodes in element ( $e$ ) and  $c_{hm}^T(t)$  are components of vector  $c_{hm}^T(t)$  defined by

$$(2.11) \quad \mathbf{c}^T(t) = \{c_{11}^T, 0, 0, 0, c_{21}^T, 0, 0, 0, c_{31}^T, 0, 0, 0, c_{41}^T, 0, 0, 0\}.$$

Also  $\Phi$  and  $\Psi$  exhibit the enriched parts of both displacement and temperature fields. They can be related to face and tip enrichment, respectively.

$$(2.12) \quad \Phi_h(x, y) = N_h(x, y)[H(x, y) - H(x_h, y_h)],$$

$$(2.13) \quad \Psi_h(x, y) = N_h(x, y) \left[ r^{0.5} \sin(\varphi/2) - r_h^{0.5} \sin(\varphi_h/2), \right. \\ \left. r^{0.5} \cos(\varphi/2) - r_h^{0.5} \cos(\varphi_h/2), \right. \\ \left. r^{0.5} \sin(\varphi) \sin(\varphi/2) - r_h^{0.5} \sin(\varphi_h) \sin(\varphi_h/2), \right. \\ \left. r^{0.5} \sin(\varphi) \cos(\varphi/2) - r_h^{0.5} \sin(\varphi_h) \cos(\varphi_h/2) \right].$$

Applying the weighted residual integral to the equation of motion (Eq. (2.1)) and the energy equation (Eq. (2.3)) with respect to the weighting functions  $S_l(x, y)$ , the formal Galerkin approximations reduce to

$$(2.14) \quad \int_{V(e)} (\sigma_{ij,j} + B_i - \rho \ddot{u}_i) S_l dV = 0, \quad l = 1, 2, \dots, ns,$$

$$(2.15) \quad \int_{V(e)} (q_{i,i} + \rho c_t \dot{\theta} + T_0 \beta \dot{\epsilon}_{ii} - R) S_l dV = 0, \quad l = 1, 2, \dots, ns,$$

where  $ns$  is the number of shape functions of the element ( $e$ ) and  $S_l$  is the component of the vector  $\mathbf{S}$

$$(2.16) \quad \mathbf{S} = \{N_1, N_2, N_3, N_4, \Phi_1, \Phi_2, \Phi_3, \Phi_4, \Psi_{1m}, \Psi_{2m}, \Psi_{3m}, \Psi_{4m}\}, \quad m = 1, 2, 3, 4.$$

By substituting Eqs. (2.4) and (2.5) into Eqs. (2.14) and (2.15) and using the Gauss divergence theorem, after some manipulations, the following equations for two-dimensional coupled thermoelasticity are obtained:

$$(2.17) \quad \int_{V(e)} \rho \ddot{u}_i S_l dV + \int_{V(e)} \frac{\partial S_l}{\partial x_j} [\mu(u_{i,j} + u_{j,i}) + \lambda u_{k,k} \delta_{ij}] dV - \int_{V(e)} \beta \theta \frac{\partial S_l}{\partial x_i} dV \\ = \int_{V(e)} B_i S_l dV + \int_{A(e)} t_i S_l dA, \quad i, j = 1, 2,$$

$$(2.18) \quad \int_{V(e)} \rho c_t \dot{\theta} S_l dV - \int_{V(e)} q_i \frac{\partial S_l}{\partial x_i} dV + \int_{V(e)} T_0 \beta \dot{u}_{i,i} S_l dV \\ = \int_{V(e)} R S_l dV - \int_{A(e)} (q_i n_i) S_l dA, \quad l = 1, 2, \dots, ns,$$

where  $t_i$  is component of traction force vector and  $ne = 4$  for a four node element. By substituting Eqs. (2.8)–(2.10) into Eqs. (2.17) and (2.18), and by assembling them into a matrix form the general finite element coupled equation is written as follows:

$$(2.19) \quad [M]\{\ddot{\Delta}\} + [C]\{\dot{\Delta}\} + [K]\{\Delta\} = \{Fr\},$$

where  $[M]$ ,  $[C]$  and  $[K]$  are the mass, damping, and stiffness matrices, respectively. Generally, for the base element ( $e$ ) which is enriched with both Heaviside and crack tip enrichment functions, these matrices can be written as follows:

$$(2.20) \quad [M]^{(e)} = \begin{bmatrix} [M_1] & [0]_{48 \times 24} \\ [0]_{24 \times 48} & [0]_{24 \times 24} \end{bmatrix},$$

$$(2.21) \quad [C]^{(e)} = \begin{bmatrix} [0]_{48 \times 48} & [0]_{48 \times 24} \\ [C_1] & [C_2] \end{bmatrix},$$

$$(2.22) \quad [K]^{(e)} = \begin{bmatrix} [K_1] & [K_2] \\ [0]_{24 \times 48} & [K_3] \end{bmatrix}.$$

$\{Fr\}$  is the force vector defined by

$$(2.23) \quad \{F\}^{(e)} = \left\{ \begin{array}{l} \int_{V(e)} [S]^T \{Bf\} dV + \int_{A(e)} [S]^T \{Tf\} dA \\ \int_{V(e)} R[St]^T dV - \int_{A(e)} (q_x n_x + q_y n_y) [St]^T dA \end{array} \right\}$$

and  $\{\Delta\}$  is the nodal displacements and temperature changes vector,

$$(2.24) \quad \{\Delta\}^{(e)} = \{a_h^u, a_h^v, b_h^u, b_h^v, c_{hm}^u, c_{hm}^v, a_h^T, b_h^T, c_{hm}^T\}^T, \quad h, m = 1, \dots, 4.$$

Also  $\{\dot{\Delta}\}$  and  $\{\ddot{\Delta}\}$  are the first and second time derivative of  $\{\Delta\}$ , respectively. Components of mass, damping, and stiffness matrices are obtained as follows:

$$(2.25) \quad [M_1] = \int_{V(e)} \rho [S]^T [S] dV,$$

$$(2.26) \quad [C_1] = \int_{V(e)} T_0 \beta [St]^T [S_1] dV,$$

$$(2.27) \quad [C_2] = \int_{V(e)} \rho c_t [St]^T [St] dV,$$

$$(2.28) \quad [K_1] = \int_{V(e)} [S_2]^T [D] [S_2] dV,$$

$$(2.29) \quad [K_2] = - \int_{V(e)} \beta [S_1]^T [St] dV.$$

For isotropic materials  $k_x = k_y = k$ , therefore  $[K_3]$  is obtained as follows:

$$(2.30) \quad [K_3] = \int_{V(e)} k [S_3]^T [S_3] dV.$$

Matrices  $[St]$ ,  $[S]$ ,  $[S_1]$ ,  $[S_2]$ ,  $[S_3]$  and vectors  $\{Bf\}$  and  $\{Tf\}$  are derived as follows:

$$(2.31) \quad [St] = [N_1 \dots N_4 \ \Phi_1 \dots \Phi_4 \ \Psi_{11} \ \Psi_{21} \ \Psi_{31} \ \Psi_{41}],$$

$$(2.32) \quad [S] = \begin{bmatrix} N_1 & \dots & N_4 & 0 & \dots & 0 & \Phi_1 & \dots & \Phi_4 & 0 & \dots & 0 \\ 0 & \dots & 0 & N_1 & \dots & N_4 & 0 & \dots & 0 & \Phi_1 & \dots & \Phi_4 \\ & & & & & & & & & \Psi_{11} & \dots & \Psi_{44} & 0 & \dots & 0 \\ & & & & & & & & & 0 & \dots & 0 & \Psi_{11} & \dots & \Psi_{44} \end{bmatrix},$$

$$(2.33) \quad [S_1] = [N_{1,x} \dots N_{4,x} \ N_{1,y} \dots N_{4,y} \ \Phi_{1,x} \dots \Phi_{4,x} \ \Phi_{1,y} \dots \Phi_{4,y} \ \Psi_{11,x} \dots \Psi_{44,x} \ \Psi_{11,y} \dots \Psi_{44,y}],$$

$$(2.34) \quad [S_2] = \begin{bmatrix} N_{1,x} & \dots & N_{4,x} & 0 & \dots & 0 & \Phi_{1,x} & \dots & \Phi_{4,x} & 0 & \dots & 0 \\ 0 & \dots & 0 & N_{1,y} & \dots & N_{4,y} & 0 & \dots & 0 & \Phi_{1,y} & \dots & \Phi_{4,y} \\ N_{1,y} & \dots & N_{4,y} & N_{1,x} & \dots & N_{4,x} & \Phi_{1,y} & \dots & \Phi_{4,y} & \Phi_{1,x} & \dots & \Phi_{4,x} \\ & & & & & & & & & \Psi_{11,x} & \dots & \Psi_{44,x} & 0 & \dots & 0 \\ & & & & & & & & & 0 & \dots & 0 & \Psi_{11,y} & \dots & \Psi_{44,y} \\ & & & & & & & & & \Psi_{11,y} & \dots & \Psi_{44,y} & \Psi_{11,x} & \dots & \Psi_{44,x} \end{bmatrix},$$

$$(2.35) \quad [S_3] = \begin{bmatrix} N_{1,x} & N_{2,x} & N_{3,x} & N_{4,x} & \Phi_{1,x} & \Phi_{2,x} & \Phi_{3,x} & \Phi_{4,x} & \Psi_{11,x} & \dots & \Psi_{44,x} \\ N_{1,y} & N_{2,y} & N_{3,y} & N_{4,y} & \Phi_{1,y} & \Phi_{2,y} & \Phi_{3,y} & \Phi_{4,y} & \Psi_{11,y} & \dots & \Psi_{44,y} \end{bmatrix},$$

$$(2.36) \quad \{Bf\} = \begin{Bmatrix} B_x \\ B_y \end{Bmatrix}, \quad \{Tf\} = \begin{Bmatrix} t_x \\ t_y \end{Bmatrix}.$$

For plane strain state matrix  $[D]$  is defined as follows:

$$(2.37) \quad [D] = \frac{E}{(1+\nu)(1-2\nu)} \begin{bmatrix} 1-\nu & \nu & 0 \\ \nu & 1-\nu & 0 \\ 0 & 0 & (1-2\nu)/2 \end{bmatrix}.$$

### 2.3. Time integration

The most widely used family of direct methods for solving semi-discrete equation of motion is the Newmark family which consists of the following equations [27]:

$$(2.38) \quad [M]\{\ddot{\Delta}_{n+1}\} + [C]\{\dot{\Delta}_{n+1}\} + [K]\{\Delta_{n+1}\} = \{Fr_{n+1}\},$$

$$(2.39) \quad \{\Delta_{n+1}\} = \{\Delta_n\} + \Delta t\{\dot{\Delta}_{n+1}\} + \Delta t^2(1/2 - \zeta)\{\ddot{\Delta}_n\} + \Delta t^2\zeta\{\ddot{\Delta}_{n+1}\},$$

$$(2.40) \quad \{\dot{\Delta}_{n+1}\} = \{\dot{\Delta}_n\} + \Delta t(1 - \gamma)\{\ddot{\Delta}_n\} + \Delta t\gamma\{\ddot{\Delta}_{n+1}\}.$$

The Newmark family contains many well-known and widely used methods. The average acceleration method, which is unconditionally stable, is one of them and it is used for structural dynamics applications. In this method,  $\gamma$  and  $\zeta$  are equal to 0.5 and 0.25, respectively. We will choose the mean acceleration scheme, which is unconditionally stable, since for the partition of unity method with an explicit Newmark-type scheme, the stable time step of the enriched problem is a small fraction of the stable time step of the problem with no enriched shape function [28].

### 3. Interaction integral and SIF computations

In this section, the interaction integral is formulated by superimposing the actual and auxiliary fields on the path independent  $J$ -integral [29]. In this work, the non-equilibrium formulation [30] is used in conjunction with the XFEM to determine the  $M$ -integral for arbitrarily oriented cracks in FGMs under thermomechanical loading and the computation of SIFs is explained in conjunction with the  $M$ -integral.

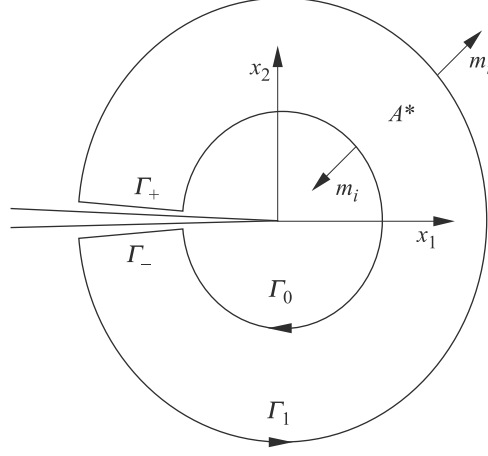
With the help of a weighting function  $q$  that is unity on  $\Gamma_0$  and zero on  $\Gamma_1$ , the  $J$  integral is written along a closed contour  $\Gamma^*$  surrounding the crack tip (as shown in Fig. 2) as [20],

$$(3.1) \quad J = \int_{\Gamma^*} \left[ \sigma_{ij} \frac{\partial u_j}{\partial x_1} - (SE + KE)\delta_{1i} \right] q m_i d\Gamma - \int_{\Gamma^+ + \Gamma^-} \sigma_{2j} \frac{\partial u_j}{\partial x_1} q d\Gamma,$$

where  $SE$  and  $KE$  are the strain energy and kinetic energy densities, respectively:

$$(3.2) \quad SE = \frac{1}{2} \sigma_{ij} (\varepsilon_{ij} - \alpha_t \theta \delta_{ij}),$$

$$(3.3) \quad KE = \frac{1}{2} \rho \dot{u}_i \dot{u}_i.$$

FIG. 2.  $J$  integral contour around the crack tip.

Assuming the traction-free condition for the cracked faces and applying the divergence theorem gives [20]

$$(3.4) \quad J = \int_{A^*} \left[ \sigma_{ij} \frac{\partial u_j}{\partial x_1} - (SE + KE) \delta_{1i} \right] \frac{\partial q}{\partial x_i} dA \\ + \int_{A^*} \left[ \frac{\partial}{\partial x_i} \left( \sigma_{ij} \frac{\partial u_j}{\partial x_1} \right) - \frac{\partial (SE + KE)}{\partial x_1} \right] q dA.$$

Substituting Eqs. (3.2) and (3.3) into Eq. (3.4) and replacing  $\sigma_{ij} u_{j,1i}$  with  $\sigma_{ij} \varepsilon_{ij,1}$  gives

$$(3.5) \quad J = \int_{A^*} \left\{ \left[ \sigma_{ij} u_{j,1} - \frac{1}{2} \sigma_{jk} \varepsilon_{jk}^m \delta_{1i} - \frac{1}{2} \rho \dot{u}_k \dot{u}_k \delta_{1i} \right] q_{,i} \right. \\ \left. + \left[ \sigma_{ij,i} u_{j,1} + \sigma_{ij} u_{j,1i} - \frac{1}{2} \sigma_{ij} \varepsilon_{ij,1}^m - \frac{1}{2} \sigma_{ij,1} \varepsilon_{ij}^m - \rho \dot{u}_i \dot{u}_{i,1} - \frac{1}{2} \rho_{,1} \dot{u}_i \dot{u}_i \right] q \right\} dA.$$

In this equation  $q$  is a weight function varying from unity at the crack tip to zero on boundary of domain  $A^*$  [30] and  $\varepsilon_{jk}^m = \varepsilon_{jk} - \varepsilon_{jk}^T$  where  $\varepsilon_{jk}$  denotes the total strain and  $\varepsilon_{jk}^m$  and  $\varepsilon_{jk}^T$  denote the mechanical part and thermal part of the strain, respectively.

Now, we consider two independent admissible fields which are the actual  $(u, \varepsilon, \sigma)$  and the auxiliary  $(u^{\text{aux}}, \varepsilon^{\text{aux}}, \sigma^{\text{aux}})$  fields. The  $J$ -integral of the superimposed fields (actual and auxiliary) can be written as follows:

$$\begin{aligned}
 (3.6) \quad J^s = \int_{A^*} \left\{ [(\sigma_{ij} + \sigma_{ij}^{\text{aux}})(u_{j,1} + u_{j,1}^{\text{aux}}) - 0.5(\sigma_{jk} + \sigma_{jk}^{\text{aux}})(\varepsilon_{jk}^m + \varepsilon_{jk}^{\text{aux}})\delta_{1i} \right. \\
 - 0.5\rho(\dot{u}_k + \dot{u}_k^{\text{aux}})(\dot{u}_k + \dot{u}_k^{\text{aux}})\delta_{1i}]q_i \\
 + [(\sigma_{ij,i} + \sigma_{ij,i}^{\text{aux}})(u_{j,1} + u_{j,1}^{\text{aux}}) + (\sigma_{ij} + \sigma_{ij}^{\text{aux}})(u_{j,1i} + u_{j,1i}^{\text{aux}}) \\
 - 0.5(\sigma_{ij} + \sigma_{ij}^{\text{aux}})(\varepsilon_{ij,1}^m + \varepsilon_{ij,1}^{\text{aux}}) - 0.5(\sigma_{ij,1} + \sigma_{ij,1}^{\text{aux}})(\varepsilon_{ij}^m + \varepsilon_{ij}^{\text{aux}}) \\
 \left. - \rho(\dot{u}_i + \dot{u}_i^{\text{aux}})(\dot{u}_{i,1} + \dot{u}_{i,1}^{\text{aux}}) - 0.5\rho_{,1}(\dot{u}_i + \dot{u}_i^{\text{aux}})(\dot{u}_i + \dot{u}_i^{\text{aux}})]q \right\} dA.
 \end{aligned}$$

Equation (3.6) is decomposed into

$$(3.7) \quad J^s = J + J^{\text{aux}} + MI,$$

where  $J$  and  $J^{\text{aux}}$  are given respectively by

$$\begin{aligned}
 (3.8) \quad J = \int_{A^*} \left\{ \left[ \sigma_{ij}u_{j,1} - 0.5\sigma_{jk}\varepsilon_{jk}^m\delta_{1i} - \frac{1}{2}\rho\dot{u}_k\dot{u}_k\delta_{1i} \right] q_i \right. \\
 \left. + [\sigma_{ij,i}u_{j,1} + \sigma_{ij}u_{j,1i} - \frac{1}{2}\sigma_{ij}\varepsilon_{ij,1}^m - \frac{1}{2}\sigma_{ij,1}\varepsilon_{ij}^m - \rho\dot{u}_i\dot{u}_{i,1} - \frac{1}{2}\rho_{,1}\dot{u}_i\dot{u}_i]q \right\} dA,
 \end{aligned}$$

$$\begin{aligned}
 (3.9) \quad J^{\text{aux}} = \int_{A^*} \left\{ \left[ \sigma_{ij}^{\text{aux}}u_{j,1}^{\text{aux}} - \frac{1}{2}\sigma_{jk}^{\text{aux}}\varepsilon_{jk}^{\text{aux}}\delta_{1i} - \frac{1}{2}\rho\dot{u}_k^{\text{aux}}\dot{u}_k^{\text{aux}}\delta_{1i} \right] q_i \right. \\
 \left. + \left[ \sigma_{ij,i}^{\text{aux}}u_{j,1}^{\text{aux}} + \sigma_{ij}^{\text{aux}}u_{j,1i}^{\text{aux}} - \frac{1}{2}\sigma_{ij}^{\text{aux}}\varepsilon_{ij,1}^{\text{aux}} - \frac{1}{2}\sigma_{ij,1}^{\text{aux}}\varepsilon_{ij}^{\text{aux}} - \rho\dot{u}_i^{\text{aux}}\dot{u}_{i,1}^{\text{aux}} - \frac{1}{2}\rho_{,1}\dot{u}_i^{\text{aux}}\dot{u}_i^{\text{aux}} \right] q \right\} dA.
 \end{aligned}$$

The resulting  $M$ -integral is given by

$$\begin{aligned}
 (3.10) \quad MI = \int_{A^*} \left\{ \left[ \sigma_{ij}u_{j,1}^{\text{aux}} + \sigma_{ij}^{\text{aux}}u_{j,1} - \frac{1}{2}\sigma_{jk}\varepsilon_{jk}^{\text{aux}}\delta_{1i} - \frac{1}{2}\sigma_{jk}^{\text{aux}}\varepsilon_{jk}^m\delta_{1i} - \rho\dot{u}_k\dot{u}_k^{\text{aux}}\delta_{1i} \right] q_i \right. \\
 + \left[ \sigma_{ij,i}u_{j,1}^{\text{aux}} + \sigma_{ij,i}^{\text{aux}}u_{j,1} + \sigma_{ij}u_{j,1i}^{\text{aux}} + \sigma_{ij}^{\text{aux}}u_{j,1i} - \frac{1}{2}\sigma_{ij}\varepsilon_{ij,1}^{\text{aux}} - \frac{1}{2}\sigma_{ij}^{\text{aux}}\varepsilon_{ij,1}^m \right. \\
 \left. - \frac{1}{2}\sigma_{ij,1}\varepsilon_{ij}^{\text{aux}} - \frac{1}{2}\sigma_{ij,1}^{\text{aux}}\varepsilon_{ij}^m - \rho\dot{u}_i\dot{u}_{i,1}^{\text{aux}} - \rho\dot{u}_i^{\text{aux}}\dot{u}_{i,1} - \rho_{,1}\dot{u}_i\dot{u}_i^{\text{aux}} \right] q \left. \right\} dA.
 \end{aligned}$$

Since the actual fields employ the quantities obtained from numerical simulation, the equilibrium and compatibility condition are satisfied. For the auxiliary

fields, the equilibrium condition is not satisfied [30], i.e.,  $\sigma_{ij,i}^{\text{aux}} \neq 0$ . While the relation between strain and displacement is compatible, i.e.,  $\varepsilon_{ij}^{\text{aux}} = \frac{1}{2}(u_{i,j}^{\text{aux}} + u_{j,i}^{\text{aux}})$  and  $\sigma_{ij}u_{j,i}^{\text{aux}} = \sigma_{ij}\varepsilon_{ij,1}^{\text{aux}}$ . The auxiliary stress field is defined as follows:

$$(3.11) \quad \sigma_{ij}^{\text{aux}} = C_{ijkl}(x)\varepsilon_{kl}^{\text{aux}}.$$

Notice that the auxiliary fields are chosen as the asymptotic fields for the homogeneous materials. Auxiliary fields, used in this paper, are based on Williams' solution [31] for stationary cracks and SWENSON and INGRAFFEA [32] for moving cracks. The resulting interaction integral ( $MI$ ) becomes

$$(3.12) \quad MI = \int_{A^*} \left\{ [\sigma_{ij}u_{j,1}^{\text{aux}} + \sigma_{ij}^{\text{aux}}u_{j,1} - \sigma_{jk}\varepsilon_{jk}^{\text{aux}}\delta_{1i} - \rho\dot{u}_k\dot{u}_k^{\text{aux}}\delta_{1i}]q_{,i} \right. \\ \left. + [\rho\ddot{u}_j u_{j,1}^{\text{aux}} + \sigma_{ij,i}^{\text{aux}}u_{j,1} + \sigma_{ij}^{\text{aux}}(\alpha_{,1}\theta + \alpha\theta_{,1})\delta_{ij} - (C_{ijkl,1}\varepsilon_{kl}^m \varepsilon_{ij}^{\text{aux}}) \right. \\ \left. - \rho\dot{u}_i\dot{u}_{i,1}^{\text{aux}} - \rho\dot{u}_i^{\text{aux}}\dot{u}_{i,1} - \rho_{,1}\dot{u}_i\dot{u}_i^{\text{aux}}]q \right\} dA.$$

Since the numerical computation of displacements, strains, stresses, etc., is based on the global coordinate system, first the  $M$ -integral is evaluated in the global ( $MI_{\text{global}}$ ) and then transformed into the local coordinate system ( $MI_{\text{local}}$ ). The global  $M$ -integral quantities are evaluated by

$$(3.13) \quad (MI_n)_{\text{global}} = \int_{A^*} \left\{ [\sigma_{ij}u_{j,n}^{\text{aux}} + \sigma_{ij}^{\text{aux}}u_{j,n} - \sigma_{jk}\varepsilon_{jk}^{\text{aux}}\delta_{ni} - \rho\dot{u}_k\dot{u}_k^{\text{aux}}\delta_{ni}] \frac{\partial q}{\partial X_i} \right. \\ \left. + [\rho\ddot{u}_j u_{j,n}^{\text{aux}} + \sigma_{ij,i}^{\text{aux}}u_{j,n} + \sigma_{ij}^{\text{aux}}(\alpha_{,n}\theta + \alpha\theta_{,n})\delta_{ij} - (C_{ijkl,n}\varepsilon_{kl}^m \varepsilon_{ij}^{\text{aux}}) \right. \\ \left. - \rho\dot{u}_i\dot{u}_{i,n}^{\text{aux}} - \rho\dot{u}_i^{\text{aux}}\dot{u}_{i,n} - \rho_{,n}\dot{u}_i\dot{u}_i^{\text{aux}}]q \right\} dA, \quad n = 1, 2,$$

where  $X_i$  denotes the global coordinate system. The local  $M$ -integral quantity is given as [30]

$$(3.14) \quad MI_{\text{local}} = (MI_1)_{\text{global}} \cos \omega + (MI_2)_{\text{global}} \sin \omega,$$

where  $\omega$  is the angle between local and global Cartesian coordinate systems on crack tip. The relation between  $M$ -integral and SIFs for stationary crack in plane strain state is as follows:

$$(3.15) \quad MI_{\text{local}} = \frac{2}{E_{\text{tip}}} (1 - \nu_{\text{tip}}^2) (K_I K_I^{\text{aux}} + K_{II} K_{II}^{\text{aux}}).$$

Also for moving crack  $MI_{\text{local}}$  can be obtained from Eq. (3.16) [8]:

$$(3.16) \quad MI_{\text{local}} = \frac{2}{E_{\text{tip}}} (1 - \nu_{\text{tip}}^2) (\beta_1(\dot{a}) K_I K_I^{\text{aux}} + \beta_2(\dot{a}) K_{II} K_{II}^{\text{aux}}),$$

where  $E_{\text{tip}}$  and  $\nu_{\text{tip}}$  denote Young's modulus and Poisson's ratio at crack tip respectively and  $\dot{a}$  is crack velocity.  $\beta_i$  are the universal functions (see [8]). Consequently,  $K_I$  and  $K_{II}$  are calculated by choosing  $K_I^{\text{aux}} = 1$ ,  $K_{II}^{\text{aux}} = 0$  and  $K_I^{\text{aux}} = 0$ ,  $K_{II}^{\text{aux}} = 1$ , respectively. The equivalent dynamic stress intensity factor  $K^{\text{eq}}$  is defined by Eq. (3.12) [8]:

$$(3.17) \quad K^{\text{eq}} = K_I \cos^3(\omega_c/2) - 1.5K_{II} \cos(\omega_c/2) \sin \omega_c,$$

where  $\omega_c$  is the direction in which the crack will propagate from its current tip, and is obtained using the maximum hoop stress criteria [8].

$$(3.18) \quad \omega_c = 2 \arctan \left( \frac{1}{4} \left[ \frac{K_I}{K_{II}} - \text{sign}(K_{II}) \left( \left( \frac{K_I}{K_{II}} \right)^2 + 8 \right)^{1/2} \right] \right), \quad -\pi < \omega_c < \pi.$$

In dynamic fracture mechanics, the initiation of growth and continued propagation of a crack depend on the equivalent stress intensity factor  $K^{\text{eq}}$  relative to the material critical stress intensity factor  $K_{IC}$ . While  $K^{\text{eq}} < K_{IC}$ , the crack tip remains stationary. If  $K^{\text{eq}} \geq K_{IC}$ , the crack tip will move. In this paper, we use an algorithm similar to the algorithm presented in reference [28] to detect the crack propagation phenomenon.

#### 4. Modeling of functionally graded layer

The material properties of the functionally graded layer must be described across the layer thickness. In the present analysis, we assume that the material gradation is along the  $x$  direction and the volume fraction of inclusion follows a simple power function,

$$(4.1) \quad V_i(x) = (x/L)^p,$$

where  $V_i$  is the volume fraction of inclusion and  $p$  is the power exponent determining the volume fraction profiles.

We assume that the functionally graded layer is made of metal-phase and ceramic-phase. In this study, we use micromechanical models for conventional composites given by HATTA and TAYA [33] and MORI and TANAKA [34] to calculate the properties of functionally graded ceramics (FGCs). Also the fracture toughness of the two-phase FGC composite needs to be determined. Here we adopt JIN and BATRA's [35] rule of mixtures formula for a two-phase FGC composite

$$(4.2) \quad K_{IC}(x) = \{V_1(x)(K_{IC}^1)^2 + V_2(x)(K_{IC}^2)^2\}^{1/2}.$$

To incorporate these relations into the XFE model, the value of each material property is calculated at each individual node based on micromechanical models.

Utilizing the generalized isoparametric graded finite elements, introduced by KIM and PAULINO [36], material properties gradation is considered in an element. In the generalized isoparametric formulation, material properties at each Gaussian integration point can be interpolated from the nodal material properties of the element using the isoparametric shape functions which are the same for the spatial coordinates and displacements. Thus, material properties such as elastic modulus ( $E$ ), Poisson's ratio ( $\nu$ ), and mass density ( $\rho$ ) at Gauss' points will be interpolated as [36]

$$(4.3) \quad E = \sum_{i=1}^m N_i E_i, \quad \nu = \sum_{i=1}^m N_i \nu_i, \quad \rho = \sum_{i=1}^m N_i \rho_i,$$

respectively, as illustrated in Fig. 3. To obtain more information about precision of this formulation, see [36].

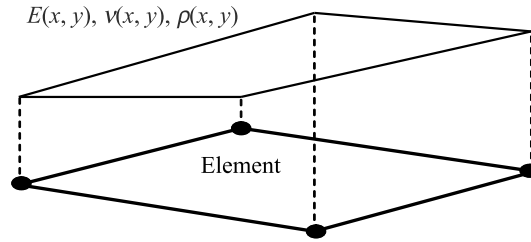


FIG. 3. Material properties variations in the generalized isoparametric formulation using the linear shape functions for the functionally graded materials.

## 5. Numerical examples

In this section, first we present three numerical examples, which examine the accuracy and precision of the presented method in this paper. Then, in the next example we consider the effect of the volume fraction profile of FGMs and loading condition on crack tip SIFs. In the last example, we study the crack propagation phenomenon in a FG layer under thermal and mechanical shocks. The plane strain state is assumed in all numerical examples.

### 5.1. Homogeneous cracked layer under thermal shock

We consider an elastic two dimensional isotropic and homogeneous layer with an edge crack (Fig. 4). The initial temperature  $T_0$  is chosen to be 400°K. The

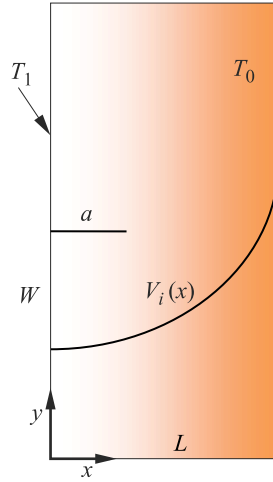


FIG. 4. Geometry and boundary condition of layer.

layer is rapidly cooled by conduction at its left surface to  $T_1$ , which is equal to  $350^\circ\text{K}$  in this study. All other sides are assumed to be thermally insulated. In this example, we neglect the coupling term in the energy equation as LEE and SIM [37] did in their analytical solution and obtained SIFs are compared with their analytical solution.

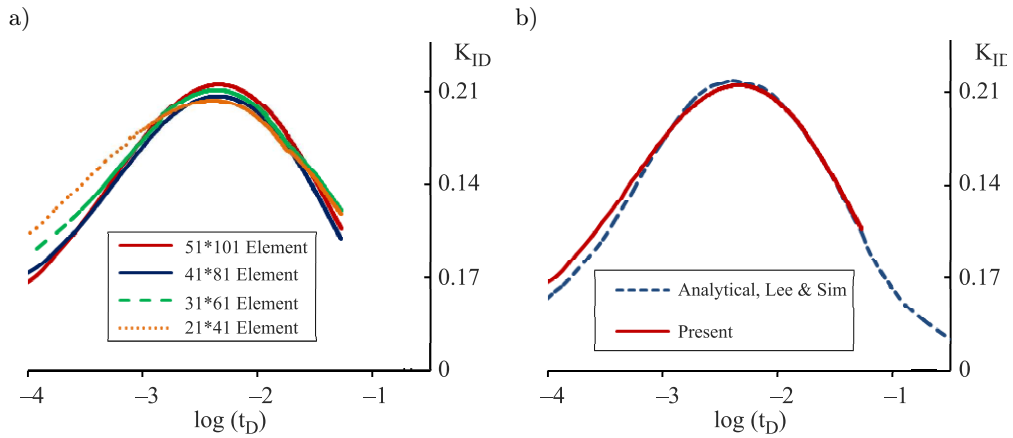


FIG. 5. Normalized SIFs versus the logarithm of normalized time for the homogeneous cracked layer: a) convergent study obtained by using different FE mesh density, b) comparison of numerical and analytical curves.

A convergent study was done by using different FE mesh density and its results were presented in Fig. 5a. This figure illustrate that a  $51 \times 101$  four-node rectangular element mesh is adequate for numerical analyzes. The analytical

and numerical dimensionless SIF ( $K_{ID}$ ) is plotted versus the logarithm of the dimensionless time ( $t_D$ ) in Fig. 5b, where good accordance is observed. In this example, we define  $K_{ID}$  and  $t_D$  which follow from Eqs. (5.1) and (5.2) [37]

$$(5.1) \quad K_{ID} = K_I(1 - \nu)/\{E\alpha(T_0 - T_1)L^{1/2}\},$$

$$(5.2) \quad t_D = kt/\rho c_t L^2.$$

### 5.2. $\text{Al}_2\text{O}_3/\text{Si}_3\text{N}_4$ FG cracked layer under thermal shock

An FG two-dimensional layer with a horizontal edge crack is considered, as shown in Fig. 4. The layer is initially at a constant temperature. Without a loss of generality, the initial temperature can be assumed to be  $200^\circ\text{K}$ . The layer is suddenly cooled down by conduction at its left surface to temperature  $T_1$ , which is equal to  $190^\circ\text{K}$ . the initial and boundary conditions for the temperature field are as follows:

$$(5.3) \quad \begin{aligned} T &= 200^\circ\text{K} && \text{at } t = 0, \\ T &= 190^\circ\text{K} && \text{at } x = 0, \\ T &= 200^\circ\text{K} && \text{at } x = L. \end{aligned}$$

It is assumed that the heat transfer coefficient on the surfaces of the FGM strip is infinite which is an idealized thermal shock boundary condition. The problem dimensions are  $L = 0.001$  m and  $W = 0.002$  m (Fig. 4). Two crack lengths are considered in this example,  $a = 0.0001$  m and  $a = 0.0003$  m. The mesh consists of  $61 \times 121$  four-node rectangular element in this example and the selected time step is  $\Delta t = 2 \times 10^{-4}$  s. A square domain with dimensions  $2a \times 2a$  was used to calculate the interaction integral and the SIF.

**Table 1. Material properties of  $\text{Al}_2\text{O}_3$  and  $\text{Si}_3\text{N}_4$  [22].**

	Young's modulus (GPa)	Poisson's ratio	CTE ( $10^{-6}/\text{K}$ )	Thermal conductivity (W/m·K)	Mass density ( $\text{Kg}/\text{m}^3$ )	Specific heat (J/Kg·K)	Fracture toughness ( $\text{MPa}\cdot\text{m}^{1/2}$ )
$\text{Al}_2\text{O}_3$	320	0.25	8	20	3800	900	4
$\text{Si}_3\text{N}_4$	320	0.25	3	35	3200	700	5

Table 1 lists the properties of the constituent materials, i.e.,  $\text{Al}_2\text{O}_3$  and  $\text{Si}_3\text{N}_4$ . This study assumes that the volume fraction of  $\text{Si}_3\text{N}_4$  (phase  $i$ ) follows a simple power function (Eq. (4.1)). The material gradation in the  $x$ -direction is considered. The SIFs for this two dimensional thermoelasticity problem are compared with those obtained by Jin and Paulino [12] in Fig. 6, which shows a good agreement between both results. Figure 6 illustrates that under thermal shock,

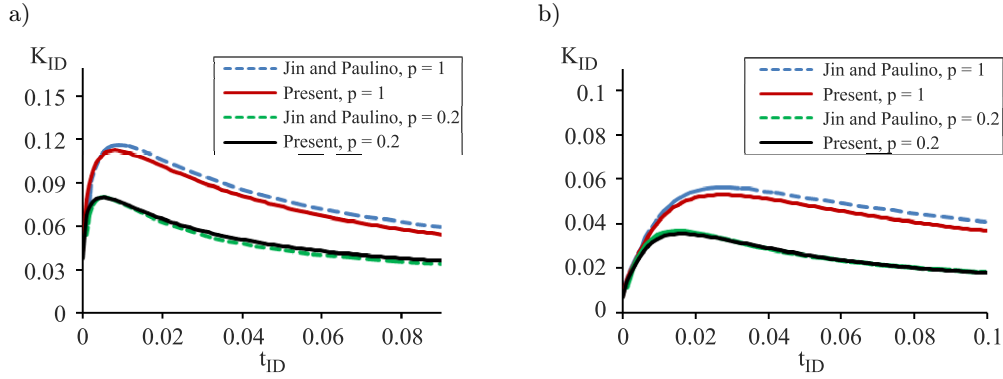


FIG. 6. Normalized SIFs versus the normalized time for  $Al_2O_3/Si_3N_4$  FG layer; a)  $a/L = 0.1$ , b)  $a/L = 0.3$ .

increasing crack length will decrease the SIF. The dimensionless thermal stress intensity factor at the crack tip and dimensionless time can be computed as follows [12].

### 5.3. Homogeneous cracked layer under mechanical shock

An elastic two-dimensional homogeneous layer with an edge crack is considered in this example. A schematic of the problem is shown in Fig. 7. A uniform traction of magnitude  $\sigma_0 = 63750$  Pa is applied at time  $t = 0$  as a step function to the top and bottom edges of the layer. The layer dimensions are  $10\text{ m} \times 4\text{ m}$ , and the initial crack length is  $a = 5\text{ m}$ . The analytical solution given by FREUND [38] is for an infinite layer. Since the specimen is finite, we stopped the simulation before the reflected wave from the edges reaches the crack tip at  $t = 0.001$  s. The material properties are  $\rho = 7833\text{ kg/m}^3$ ,  $E = 200\text{ GPa}$  and  $\nu = 0.3$ . A  $201 \times 81$  quadrilateral mesh was used for discretizing the layer.

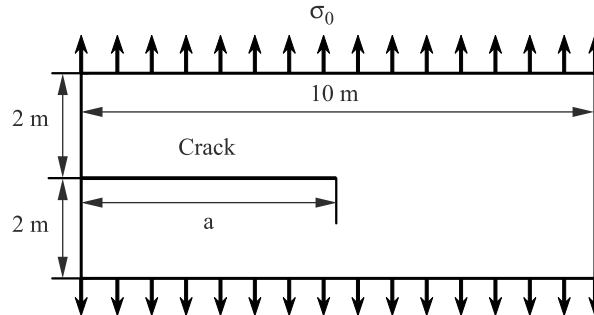


FIG. 7. Isotropic and homogeneous cracked layer under mechanical shock.

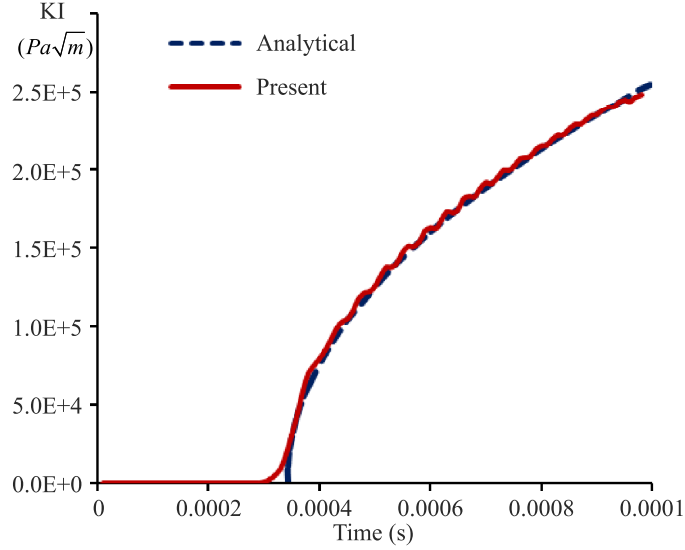


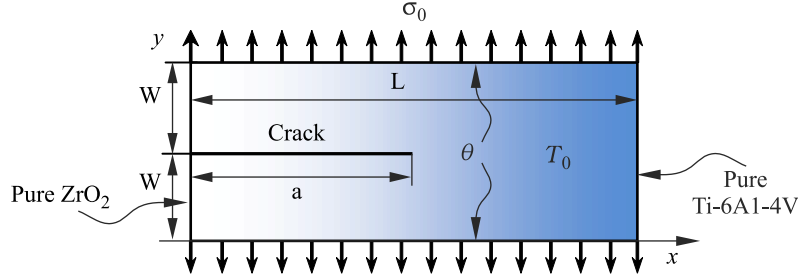
FIG. 8. Comparison of numerical and analytical SIFs for homogeneous cracked layer under mechanical shock.

We use a domain of  $0.5 \text{ m} \times 0.5 \text{ m}$  to calculate the interaction integral and SIF. The SIF values for this problem are obtained and compared with the analytical solution in Fig. 8, which shows a good agreement between both results. The results are quite smooth and oscillate close to the analytic solution. These unavoidable oscillations are also observed in [39, 5, 40, 20, 21] for the standard XFEM. These oscillations are the characteristic of the solution of a shock propagation problem by the FE discretization in the spatial domain and by the Newmark method in the time domain [21].

#### 5.4. Ti-6Al-4V/ZrO<sub>2</sub> FG cracked layer under thermo-mechanical shock

An elastic two-dimensional FG layer with an edge crack (Fig. 9) is considered in this example. A tension of magnitude  $\sigma_0 = 10 \text{ MPa}$  and cooling thermal shocks of magnitude  $\theta = -10$  and  $\theta = -20$  is applied at time  $t = 0$  as a step function to the top and bottom edges. The layer dimensions are  $L = 0.1 \text{ m}$  and  $W = 0.02 \text{ m}$ , and the initial crack length is  $a = 0.05 \text{ m}$ . The calculations are carried out to the point  $t = 10 \text{ }\mu\text{s}$ , before the reflected wave from the edges reaches the crack tip. Initial temperature  $T_0$  is chosen to be  $300^\circ\text{K}$ .

In these numerical calculations, we consider a Ti-6Al-4V and ZrO<sub>2</sub> FGM. The properties of the constituent materials are presented in Table 2. The material gradation in the  $x$ -direction is considered and the volume fraction of ZrO<sub>2</sub> follows then Eq. (4.1). A mesh with  $81 \times 201$  four-node rectangular element is used and

FIG. 9. Ti-6Al-4V/ZrO<sub>2</sub> FG cracked layer under thermo-mechanical shock.**Table 2.** Material properties of Ti-6Al-4V and ZrO<sub>2</sub> [21].

	Young's modulus (GPa)	Poisson's ratio	CTE (10 <sup>-6</sup> /K)	Thermal conductivity (W/m·K)	Mass density (Kg/m <sup>3</sup> )	Specific heat (J/Kg·K)	Fracture toughness (MPa·m <sup>1/2</sup> )
Ti-6Al-4V	66.2	0.321	10.3	18.1	4410	808.3	60
ZrO <sub>2</sub>	117	0.333	7.11	2.036	5600	615.6	4

the selected time step is  $\Delta t = 10^{-7}$  s. A domain of dimensions  $0.005 \text{ m} \times 0.005 \text{ m}$  was used to calculate the SIF.

To study the effect of the material gradation, the coupled thermoelasticity problem with three different values of  $p$  is analyzed (i.e.,  $p = 0.2$ ,  $p = 1$  and  $p = 5$ ). The time variations of the mode-I thermal dynamic SIF are shown in Fig. 10.

Figures 10a and 10b demonstrate that the SIF due to thermomechanical shocks is superposition of SIFs produced with thermal and mechanical shocks separately. Figures 10c and 10d show that a rise in the material gradient parameter  $p$  increases the SIF regardless of loading conditions. We can see from Fig. 10 that the curve related to the thermal shocks is smoother than other curves.

### 5.5. Crack propagation phenomenon in the Ti-6Al-4V/ZrO<sub>2</sub> FG layer

In this example, we study the crack propagation phenomenon in a FG layer with a horizontal edge crack under thermal and mechanical shocks. Dimensions, properties, mesh and boundary conditions of considered layer are identical to the previous example. Initial temperature  $T_0$  is chosen to be  $500^\circ\text{K}$ . A cooling thermal shock equal to  $-100$  degree ( $\theta = -100$ ) and a mechanical shock of magnitude  $\sigma_0 = 200 \text{ MPa}$  are applied to upper and bottom surfaces of layer. The total simulation time is  $60 \mu\text{s}$ .

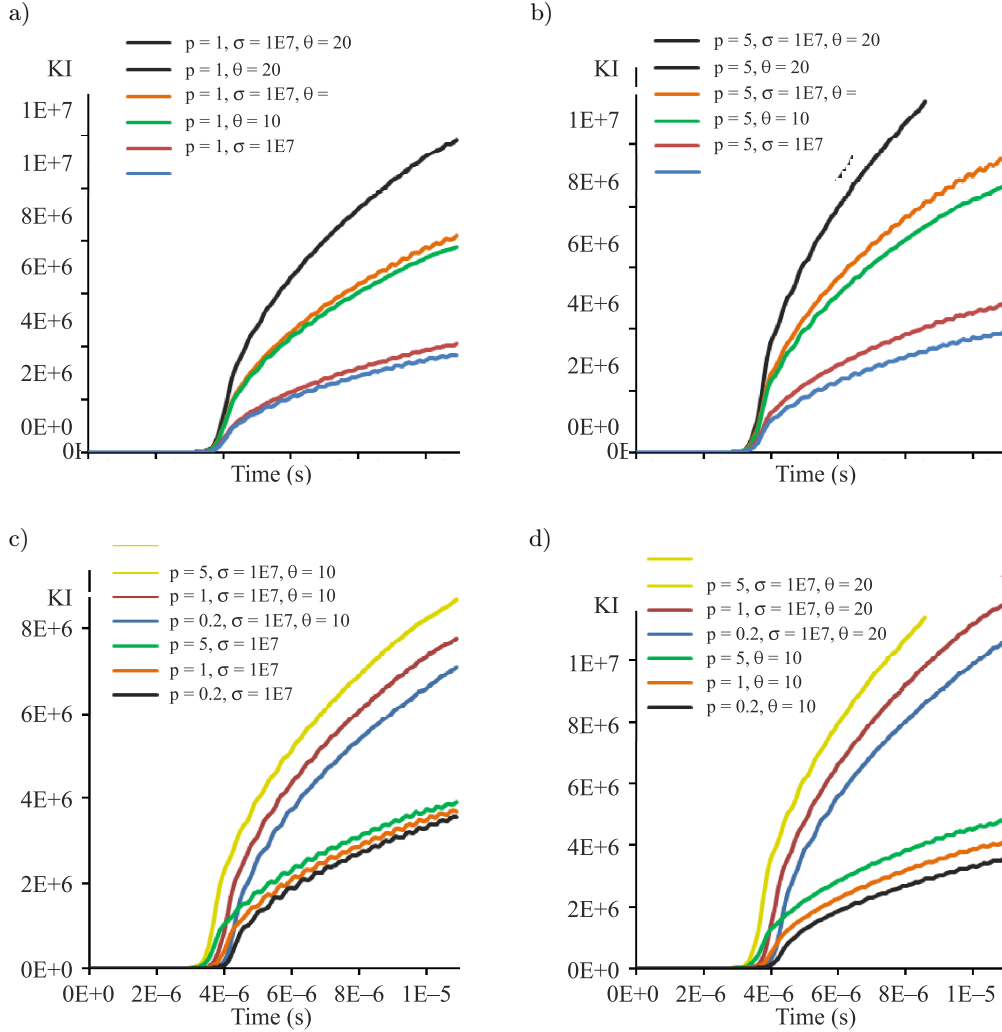


FIG. 10. Stress intensity factor versus time for the Ti-6Al-4V/ZrO<sub>2</sub> FG cracked layer in various loading conditions: a)  $p = 1$ , b)  $p = 5$ , c) mechanical and thermomechanical shock, d) thermal and thermomechanical shock.

The crack tip propagation velocity curves for FG layers with  $p = 0.2$  and  $p = 5$  under thermomechanical shocks are illustrated in Fig. 11. It is derived from Fig. 11 that crack propagation initiation time is dependent on the loading condition and the volume fraction profile of the FG layer. Crack growth initiation under mechanical shocks happens earlier than crack growth initiation under thermal shocks. Also a rise in the material gradient parameter  $p$  decreases the crack propagation initiation time and increases the crack propagation velocity.

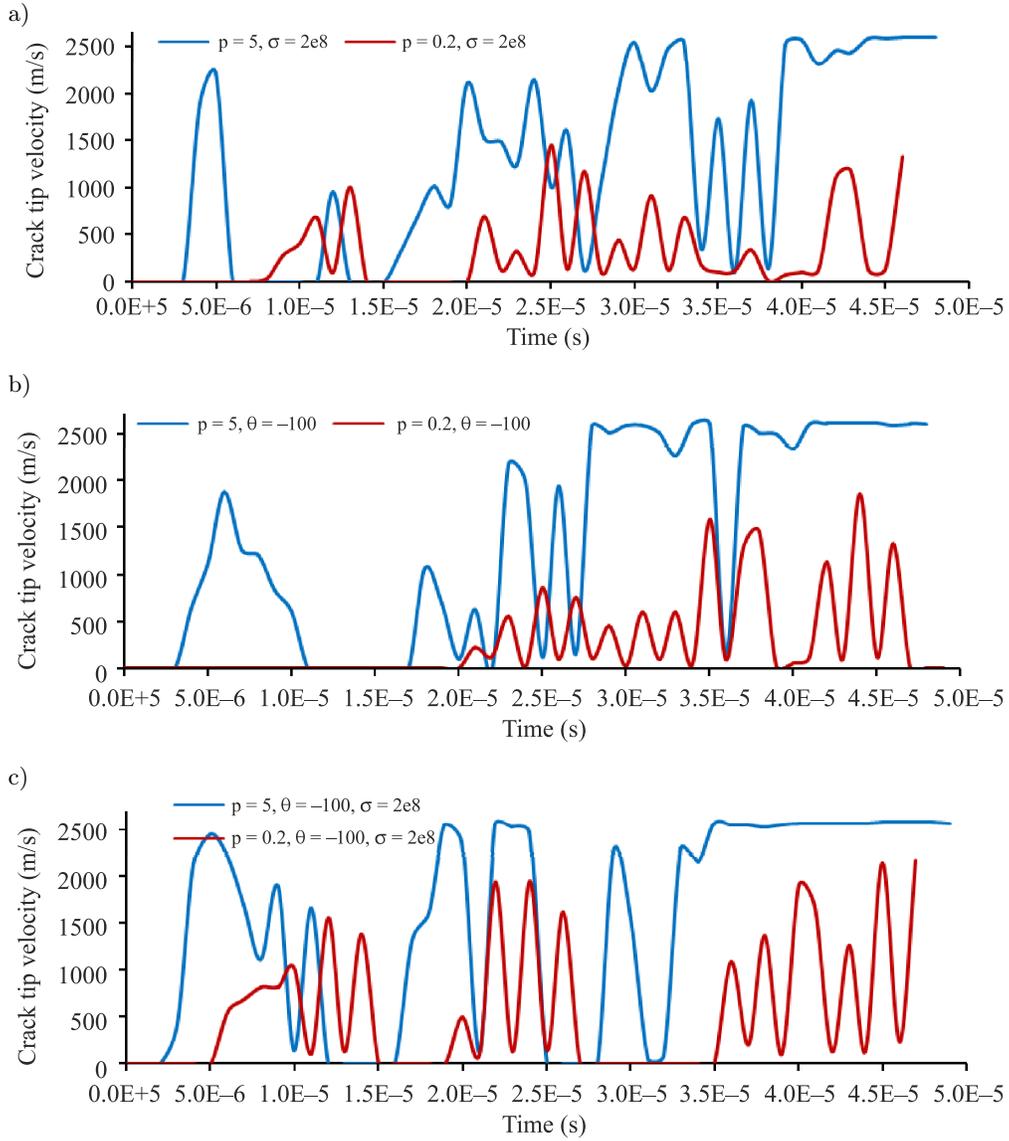


FIG. 11. Crack tip velocity for the Ti-6Al-4V/ZrO<sub>2</sub> FG layers under: a) mechanical shock, b) thermal shock, c) thermomechanical shock.

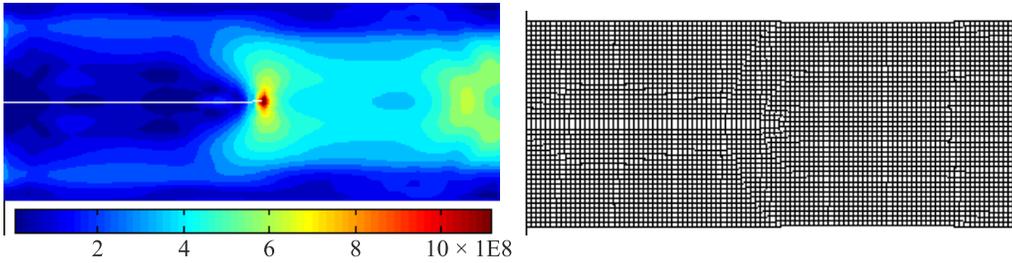
Figure 11 shows that the velocity curve related to  $p = 5$  almost lies over curve related to  $p = 0.2$ .

Figures 12 and 13 illustrate the crack propagation path, von Mises stress contours and deformed mesh for FG layers with  $p = 0.2$  and  $p = 5$  respectively, under thermomechanical shocks at various times. For more clarification, displace-

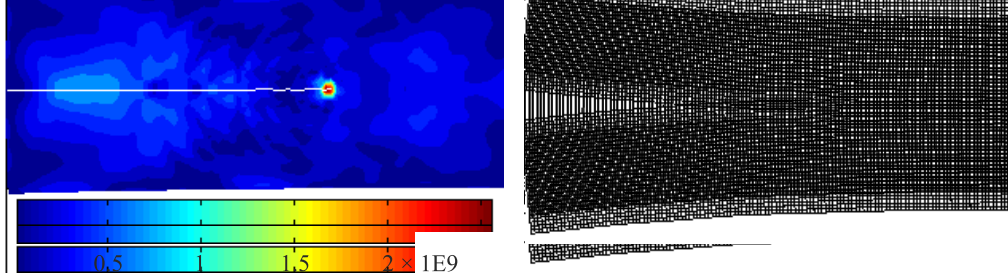
ments were multiplied by 5 in plotting deformed meshes. Figures 12 and 13 show that crack propagates in straight line until about  $t = 40 \mu\text{s}$ , regardless of loading conditions and material gradient parameter ( $p$ ). After this time crack deviates upward. BELYTSCHKO *et al.* [5] predicted for homogeneous materials that after crack propagation in straight line, crack branching may be occur but our written code does not have ability to detect the crack branching phenomenon.

Comparison of Figs. 12 and 13 confirms that increasing  $p$  will increase crack propagation velocity and crack length. In addition, deviation of crack path will increase with increasing  $p$ .

a)  $t = 10 \mu\text{s}$



b)  $t = 40 \mu\text{s}$



c)  $t = 60 \mu\text{s}$

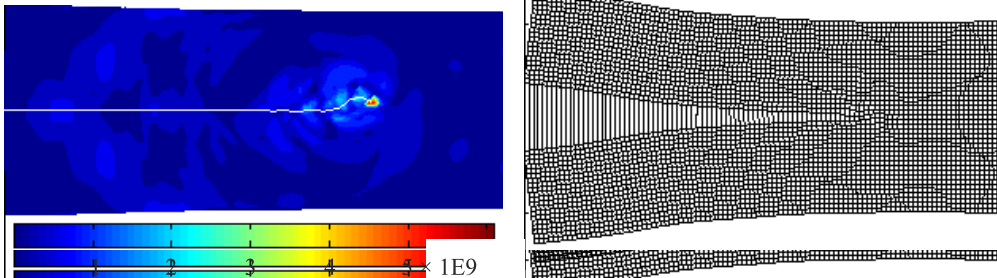


FIG. 12. Von Mises stress contours and deformed mesh of Ti-6Al-4V/ZrO<sub>2</sub> FG layer with  $p = 0.2$  under thermomechanical shock at various times. Von Mises stress contours and deformed mesh of Ti-6Al-4V/ZrO<sub>2</sub> FG layer with  $p = 0.2$  under thermomechanical shock at various times.

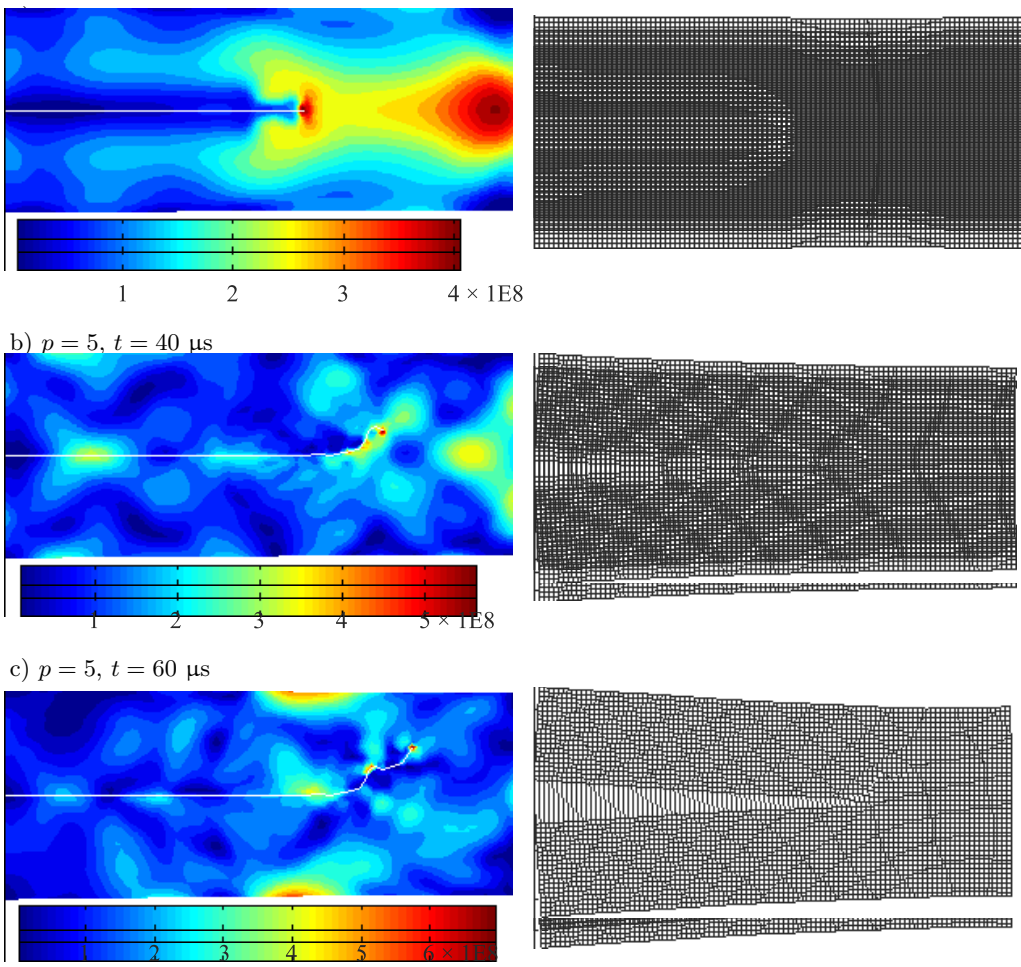


FIG. 13. Von Mises stress contours and deformed mesh of Ti-6Al-4V/ZrO<sub>2</sub> FG layer with  $p = 5$  under thermomechanical shock at various times.

## 6. Conclusions

In this study, classical coupled thermoelastic equations were solved using the XFE and Newmark’s methods in FGMs. The most general form of interaction integral were developed to evaluate dynamical SIFs for both homogenous and FG materials. In addition, the crack propagation phenomenon was considered in FG layers under thermomechanical shock. Some numerical examples were implemented and good agreements and accuracies were observed. The following results were obtained for the Ti-6Al-4V/ZrO<sub>2</sub> FG layer where the crack is located on the stiffer side:

1. A rise in the material gradient parameter ( $p$ ) increases the SIF (KI).
2. The crack growth initiation under mechanical shocks happens earlier than the crack growth initiation under thermal shocks.
3. An increase in the material gradient parameter ( $p$ ) decreases the crack propagation initiation time.
4. A rise in the material gradient parameter ( $p$ ) increases the crack propagation velocity.

## References

1. T. BLACK, T. BELYTSCHKO, *Elastic crack growth in finite elements with minimal remeshing*, Int. J. Numer. Method Engin., **45**, 601–620, 1999
2. N. MOËS, J. DOLBOW, T. BELYTSCHKO, *A finite element method for crack growth without remeshing*, Int. J. Numer. Method Engin., **46**, 1, 131–150, 1999.
3. T. BELYTSCHKO, N. MOËS, S. USUI, C. PARIMI, *Arbitrary discontinuities in finite elements*, Int. J. Numer. Method Engin., **50**, 4, 993–1013, 2001.
4. J.M. MELENK, I. BABUŠKA, *The partition of unity finite element method: basic theory and applications*, Comput. Method in Appl. Mech. and Engin., **139**, 1-4, 289–314, 1996.
5. T. BELYTSCHKO, H. CHEN, J. XU, G. ZI, *Dynamic crack propagation based on loss of hyperbolicity and a new discontinuous enrichment*. Int. J. for Num. Methods in Engin. **58**, 1873–1905, 2003.
6. P. ROZYCKI, N. MOËS, E. BÉCHET, C. DUBOIS, *X-FEM explicit dynamics for constant strain elements to alleviate mesh constraints on internal or external boundaries*, Comput. Method Appl. Mech. Eng., **197**, 5, 349–363, 2008.
7. C. LINDER, F. ARMERO, *Finite elements with embedded branching*, Finite Elements in Analysis and Design, **45**, 280–293, 2009.
8. T. MENOULLARD, J.-H. SONG, Q. DUAN, T. BELYTSCHKO, *Time dependent crack tip enrichment for dynamic crack propagation*, Int. J. of Fract., **162**, 33–49, 2010.
9. N. NODA, *Thermal stress intensity factor for functionally gradient plate with an edge crack*, J. Therm. Stresses, **20**, 3-4, 373–387, 1997.
10. T. FUJIMOTO, N. NODA, *Crack propagation in a functionally graded plate under thermal shock*, Arch. Appl. Mech., **70**, 6, 377–386, 2000.
11. T. FUJIMOTO, N. NODA, *Two crack growths in a functionally graded plate under thermal shock*, J. Therm. Stresses, **24**, 847–862, 2001.
12. Z.-H. JIN, G.H. PAULINO, *Transient thermal stress analysis of an edge crack in a functionally graded material*, Int. J. of Fract., **107**, 73–98, 2001.
13. CH. ZHANG, J. SLADEK, V. SLADEK, *Effects of Material Gradients on Transient Dynamic Mode-III Stress Intensity Factors*. International Journal of Solids and Structures, **40**, 5251–5270, 2003.
14. H.M. XU, X.F. YAO, X.O. FENG, H.-Y. YEH, *Dynamic stress intensity factors of a semi-infinite crack in an orthotropic functionally graded material*, Mechanics of Materials, **40**, 1, 37–47, 2008.

15. P. HOSSEINI-TEHRANI, M.R. ESLAMI, H.R. DAGHYANI, *Dynamic crack analysis under coupled thermoelastic assumption*, J. Appl. Mech., **68**, 4, 584–588, 2001.
16. P. HOSSEINI-TEHRANI, A.R. HOSSEINI-GODARZI, M. TAVANGAR, *Boundary element analysis of stress intensity factor KI in some two-dimensional dynamic thermoelastic problems*, Eng. Anal. B. E., **29**, 232–240, 2005.
17. M. DUFLOT, *The extended finite element method in thermoelastic fracture mechanics*, Int. J. Num. Meth. Engin., **74**, 827–847, 2008.
18. A. KC, J.-H. KIM, *Interaction integrals for thermal fracture of functionally graded materials*, Engin. Fract. Mech., **75**, 2542–2565, 2008.
19. H. WANG, Q.H. QIN, *Meshless approach for thermo-mechanical analysis of functionally graded materials*, Engin. Analy. Boundary Elem., **32**, 9, 704–712, 2008.
20. A. ZAMANI, M.R. ESLAMI, *Coupled dynamical thermoelasticity of a functionally graded cracked layer*, J. Therm. Stresses, **32**, 969–985, 2009.
21. A. ZAMANI, M.R. ESLAMI, *Implementation of the extended finite element method for dynamic thermoelastic fracture initiation*, Int. J. Solid Struc., **47**, 1392–1404, 2010.
22. Y. FENG, Z. JIN, *Thermal fracture of functionally graded plate with parallel surface cracks*, Acta Mechanica Solida Sinica, **22**, 5, 453–464, 2009.
23. A.V. EKHLAKOV, O.M. KHAY, CH. ZHANG, J. SLADEK, V. SLADEK, *A BDEM for transient thermoelastic crack problems in functionally graded materials under thermal shock*, Comp. Mater. Scie., **57**, 30–37, 2012.
24. A.V. EKHLAKOV, O.M. KHAY, CH. ZHANG, J. SLADEK, V. SLADEK, X.W. GAO, *Thermoelastic crack analysis in functionally graded materials and structures by a BEM*, Fatig. & Fract. Engin. Mater. & Struct., **35**, 8, 742–766, 2012.
25. R.B. HETNARSKI, M.R. ESLAMI, *Thermal Stresses – Advanced Theory and Applications*, Springer, 2009.
26. S. MOHAMMADI, *Extended Finite Element Method*, Blackwell Publishing Ltd, 2008.
27. T. JR. HUGHES, *The finite element method*, Englewood Cliffs, New Jersey, Prentice-Hall INC. 1987.
28. C.A. GERLACH, *Computational methods for the dynamic response of cracked specimens*, Ph.D Thesis, Northwestern university, Evanston, Illinois, 1999.
29. J.R. RICE, *A path-independent integral and the approximate analysis of strain concentration by notches and cracks*, ASME J. Appl. Mech., **35**, 2, 379–386, 1968.
30. S.H. SONG, G.H. PAULINO, *Dynamic stress intensity factors for homogeneous and smoothly heterogeneous materials using the interaction integral method*, Int. J. Solid Struc., **43**, 4830–4866, 2006.
31. M.L. WILLIAMS, *On the stress distribution at the base of a stationary crack*, ASME J. Appl. Mech., **24**, 1, 109–114, 1957.
32. D.V. SWENSON, A.R. INGRAFFEA, *Modeling mixed-mode dynamic crack propagation using finite elements: theory and applications*, comp. mech., **3**, 381–397, 1988.
33. H. HATTA, M. TAYA, *Equivalent inclusion method for steady state heat conduction in composites*, Int. J. Engin. Scie., **24**, 520–524, 1986.

34. T. MORI, K. TANAKA, *Average stress in matrix and average elastic energy of materials with misfitting inclusions*, Acta Materialia, **21**, 571–574, 1973.
35. Z.-H. JIN, R.C. BATRA, Some basic fracture mechanics concepts in functionally graded materials, J. Mech. Phys. Solid, **44**, 1221–1235, 1996.
36. J.-H. KIM, G.H. PAULINO, *Isoparametric graded finite elements for nonhomogeneous isotropic and orthotropic materials*, ASME J. Appl. Mech., **69**, 502–514, 2002.
37. K.Y. LEE, K.B. SIM, *Thermal shock stress intensity factor by Bueckner’s weight function method*, Engin. Frac. Mech., **37**, 4, 799–804, 1990.
38. L.B. FREUND, *Dynamic Fracture Mechanics*, Cambridge University Press, Cambridge, 1990.
39. C.A. DUARTE, O.N. HAMZEH, T.J. LISZKA, W.W. TWORZYDLO, *A generalized finite element method for the simulation of three dimensional dynamic crack propagation*. Computer Methods in Applied Mechanics and Engineering, **190**, 2227–2262, 2001.
40. J. RÉTHORÉ, A. GRAVOUIL, A. COMBESURE, *An energy-conserving scheme for dynamic crack growth using extended finite element method*, Int. J. for Num. Methods in Engin., **63**, 631–659, 2005.

Received August 13, 2012; revised version December 27, 2012.

---